

006405

---

**Investigation of Hydrophobic Interactions  
in Colloidal and Biological Systems by  
Molecular Dynamics Simulations and  
NMR Spectroscopy**

---

**M. H. Alaimo and T. F. Kumosinski**

U.S. Department of Agriculture, Agricultural Research Service,  
Eastern Regional Research Center, 600 East Mermaid Lane,  
Wyndmoor, Pennsylvania 19038

# Investigation of Hydrophobic Interactions in Colloidal and Biological Systems by Molecular Dynamics Simulations and NMR Spectroscopy

M. H. Alaimo and T. F. Kumosinski\*

U.S. Department of Agriculture,<sup>†</sup> Agricultural Research Service, Eastern Regional Research Center, 600 East Mermaid Lane, Wyndmoor, Pennsylvania 19038

Received November 4, 1996. In Final Form: January 27, 1997<sup>⊗</sup>

Interactions of hydrophobic molecular domains determine many of the functional properties of food proteins and colloidal food aggregates, such as emulsification, gelation, and foaming ability. A molecular basis for macromolecular interactions and conformational stability is established through investigation of simple model systems. Molecular modeling and dynamics simulations have been used to study the role of hydrophobic interaction forces in driving the formation of model amphiphile aggregate systems. An approximation to hydrophobic attraction between hydrocarbon tails was required to achieve stable, dynamic aggregate models for Aerosol-OT (AOT)/water/oil microemulsions, micelles of AOT in water, and a stacked AOT/*para*-chlorophenol gel in either CCl<sub>4</sub> or benzene. One- and two-dimensional NMR spectroscopic methods have been used to characterize the pH and temperature dependent conformational changes in the model polypeptide poly(L-lysine). Changes in proton chemical shifts and line widths indicate that the backbone mobility of poly(L-lysine) is not greatly diminished by the coil-helix transition. ROESY and transverse-ROESY couplings, as well as  $T_1$  and  $T_2$  relaxation measurements, suggest that lysyl side chain mobility remains largely unrestricted upon formation of periodic secondary structure. Molecular dynamics simulations of poly(L-lysine) conformers substantiate the importance of hydrophobic side chain domains in stabilizing secondary structural features in aqueous solution.

## Introduction

Hydrophobic interaction forces play a considerable role in the self-assembly of surfactant aggregates such as micelles, vesicles, and microemulsion droplets. In biological systems, hydrophobic interactions are central to such important processes as lipid bilayer formation and determining protein conformation and folding patterns. There have been several extensive treatments of the subject.<sup>1,2</sup> The functionality of foods is often governed by physical processes and interaction of food components. An understanding of hydrophobic interactions is essential to food science and technology, as these forces control the formation of numerous food emulsions and dispersions and help to stabilize food protein conformation.

In recent years, direct measurement of the long-range forces between hydrophobic surfaces has been the subject of a number of reports.<sup>3-10</sup> Strongly attractive forces between macroscopic hydrophobic surfaces in water are observed, often exceeding anticipated van der Waals forces by up to two orders of magnitude. These dramatic results,

obtained using Israelachvili's surface force apparatus (SFA),<sup>11</sup> have been corroborated using atomic force microscopy (AFM).<sup>12-14</sup> The force between hydrophobic surfaces has been shown to decay exponentially with distance<sup>3-10</sup> as opposed to following the power-law behavior of continuum theory, while some results give better fits to a double exponential.<sup>10,12</sup> Despite the profusion of experimental evidence to hydrophobic attraction, the precise origins of this force remain undetermined.

As the early concept of a "hydrophobic bond"<sup>15</sup> has never been substantiated on a theoretical basis, hydrophobic interactions are often justified simply by the gain in free energy upon removal of water molecules from the hydrocarbon interlayer. However, the magnitude of these forces compels an explanation based on surface interactions rather than water structural effects. Mechanisms have been proposed based upon vapor cavitation<sup>16</sup> and Debye-screened dipole-dipole correlations.<sup>17</sup> While the latter proposal explains the exponential decay of the interaction, neither model accounts for the magnitude and range of measured forces.

Attractive forces between hydrophobic surfaces have been characterized to some extent on a qualitative basis. In studies involving monolayers of surfactant deposited on mica surfaces, attractive forces between two surfaces in water were dependent upon alkyl chain length and temperature.<sup>10</sup> At low temperatures attractive forces increased with chain length, while in all cases surface attraction diminished dramatically with heating. Additionally, measured forces depended strongly on the state

\* To whom correspondence should be addressed.

<sup>†</sup> Mention of brand or firm names does not constitute an endorsement by the U.S. Department of Agriculture over others of a similar nature not mentioned.

<sup>⊗</sup> Abstract published in *Advance ACS Abstracts*, March 15, 1997.

(1) Tanford, C. *The Hydrophobic Effect*, 2nd ed.; Wiley: New York, 1980.

(2) Israelachvili, J. N. *Intermolecular and Surface Forces*, 2nd ed.; Academic: New York, 1991.

(3) Israelachvili, J. N.; Pashley, R. M. *Nature* **1982**, *300*, 341-342.

(4) Israelachvili, J. N.; Pashley, R. M. *J. Colloid Interface Sci.* **1984**, *98*, 500-514.

(5) Pashley, R. M.; McGuiggan, P. M.; Ninham, B. W.; Evans, D. F. *Science* **1985**, *229*, 1088-1089.

(6) Claesson, P. M.; Blom, C. E.; Herder, P. C.; Ninham, B. W. *J. Colloid Interface Sci.* **1986**, *114*, 234-242.

(7) Claesson, P. M.; Christenson, H. K. *J. Phys. Chem.* **1988**, *92*, 1650-1655.

(8) Christenson, H. K.; Fang, J.; Ninham, B. W.; Parker, J. L. *J. Phys. Chem.* **1990**, *94*, 8004-8006.

(9) Kurihara, K.; Kato, S.; Kunitake, T. *Chem. Lett.* **1990**, *9*, 1553-1558.

(10) Tsao, Y.-H.; Yang, S. X.; Evans, D. F.; Wennerström, H. *Langmuir* **1991**, *7*, 3154-3159.

(11) Israelachvili, J. N.; Adams, G. E. *J. Chem. Soc., Faraday Trans. 1* **1978**, *74*, 975-1001.

(12) Tsao, Y.-H.; Evans, D. F.; Wennerström, H. *Science* **1993**, *262*, 547-550.

(13) Rabinovich, Y. A.; Yoon, R.-H. *Langmuir* **1994**, *10*, 1903-1909.

(14) Mantel, M.; Rabinovich, Y. A.; Wightman, J. P.; Yoon, R.-H. *J. Colloid Interface Sci.* **1995**, *170*, 203-214.

(15) Kauzmann, W. *Adv. Protein Chem.* **1959**, *14*, 1-63.

(16) Christenson, H. K.; Claesson, P. M. *Science* **1988**, *239*, 390-395.

(17) Attard, P. *J. Phys. Chem.* **1989**, *93*, 6441-6444.

of the hydrocarbon chains on the surface. Results showed that the attraction is greater between surfaces having hydrophobic layers with a high degree of crystalline order, while measured forces were smaller and decay lengths shorter for surfaces with surfactant layers in a liquid crystal or partially disordered state. These properties were observed in both water and ethylene glycol and cannot be attributed solely to the molecular properties of water.<sup>12</sup> A similar study on monolayer-coated surfaces revealed that long-range attraction was higher for surfaces coated with double-chain surfactants.<sup>7</sup> Surprisingly enough, attractive properties of disparate hydrophobic surfaces (as determined by SFA analysis) show little correlation with their bulk surface hydrophobicity, as determined by conventional measurements of adhesion and the advancing contact angle of water.<sup>8</sup> In general, local molecular structure seems to dictate the magnitude of measured hydrophobic attractive forces, with cases notably exceeding predicted van der Waals dispersive forces occurring only for highly ordered alkyl chains in an *all-trans* (solid-like) configuration.

Molecular dynamics simulations have emerged as an important tool for interpreting the structure and interaction of supramolecular systems, owing largely to improvements in computational power and available software. In a recent report, simulations of surfactant bilayer and micelle self-assembly included an approximation to hydrophobic attraction.<sup>18</sup> Hydrophobic attractive forces were approximated by multiplying the normally accepted van der Waals attraction between hydrocarbon chains of surfactants by factors necessary to mimic experimentally derived forces. Dynamic structures were simulated which closely resemble models derived from experimental data. Without some approximation of hydrophobic forces, stable surfactant aggregates were not attainable during the course of dynamics simulations. In this study, we have extended this approach to several model systems significant to food chemistry, including water-in-oil microemulsions, organogels, and hydrophobic polypeptides, with an emphasis on determining the role of local molecular structure in maintaining stable aggregate systems.

Molecular interactions in foods are driven by the total of a variety of forces including hydrogen bonding, hydrophobic interactions, and electrostatic forces of both ionic and dipolar (van der Waals) character. Foods are highly complex systems. Most foods include polymeric protein and starch structures and monomeric phases of water and fat, in varying degrees of solidity or liquidity. The compositional and dynamic complexity of foods must be approached systematically. Model systems are often desired to elucidate the underlying physical and chemical processes.

Two important food dispersions are emulsions and gels. Many food products, such as mayonnaise and salad dressings, are emulsions. Biopolymer gels are often formed by food additives such as carrageenan, starch, and pectin. Water-in-oil microemulsions formulated with the surfactant sodium bis(2-ethylhexyl)sulfosuccinate, or Aerosol-OT (AOT), in a diversity of nonpolar media have been widely studied,<sup>19</sup> in part due to its ability to form simple three-component reverse micelles without using a cosurfactant. A water/AOT/toluene assembly has been modeled in this study to demonstrate the effect of an empirical long-range hydrophobic force on the stability of microemulsions. Micelles of AOT in water will also be discussed. Adding gelatin to AOT microemulsions can

lead to gelation under certain conditions.<sup>20</sup> A series of recent papers described a novel organogel formed by the addition of a phenolic component to AOT in hydrocarbons.<sup>21–23</sup> The systems exhibit a sharp liquid–gel phase transition as a function of hydration, which may serve as a good model for the diversity of hydrated gels in food materials and additives. Molecular dynamics simulations will be presented, indicating the importance of a hydrophobic force between alkyl chains in maintaining the “stacked” phenolic microstructure.

The interaction of proteins with other proteins and food components greatly influences the bulk properties of the final product, including texture, taste, and appearance. The relationship of protein functionality to food and food ingredient utilization is of great interest. Poly(L-lysine) is often used as a model protein because of its ability to adopt three distinct secondary structures:  $\alpha$ -helix,  $\beta$ -sheet, and the unordered “random coil”. NMR spectroscopy has emerged in the past two decades as one of the most efficacious techniques for determining the structure and function of proteins.<sup>24</sup> A generation of two-dimensional NMR techniques has been developed, dramatically improving spectral resolution and correlating power.<sup>25</sup> Structures derived from NMR constraints are often refined using molecular dynamics<sup>26</sup> and simulated annealing.<sup>27</sup> Molecular dynamics and experimental NMR will be used to demonstrate the importance of hydrophobic interactions to the conformational stability of poly(L-lysine).

## Experimental Section

**Molecular Modeling.** Polypeptides and surfactant aggregate structures were constructed on an Evans and Sutherland PS390 interactive computer graphics display driven by Tripos Sybyl (Tripos Assoc., Inc., St. Louis, MO) molecular modeling software on a Silicon Graphics Indigo UNIX-based workstation. Polypeptides and polypeptide aggregate structures were constructed in the Tripos force field.<sup>28</sup> Surfactant aggregates were assembled from component monomers in the Tripos force field using a docking procedure. Solvent molecules were added to molecular models using the Silverware algorithm.<sup>29</sup>

**Energy Minimization.** Structure–function relationships for small molecules can be explored using quantum mechanical calculations (e.g. *ab initio* calculations) by determining, for instance, lowest potential energy versus geometry. The study of systems of biological interest such as protein aggregates, however, still demands elementary model empirical energy functions. Although molecular force field functions are somewhat crude, they have been applied successfully to the study of hydrocarbons, oligonucleotides, polysaccharides, peptides, and proteins.<sup>30</sup> Molecular mechanics or force field methods employ a combination of potential energy functions to determine an optimum structure. The concept, equation for, and full description of a molecular force field were given in a previous com-

(20) Atkinson, P. J.; Robinson, B. H.; Howe, A. M.; Pitt, A. R. *Colloids Surf. A* **1995**, *94*, 231–242.

(21) Xiaodong, X.; Ayyagari, M.; Tata, M.; John, V. T.; McPherson, G. L. *J. Phys. Chem.* **1993**, *97*, 11350–11353.

(22) Tata, M.; John, V. T.; Waguespack, Y. Y.; McPherson, G. L. *J. Phys. Chem.* **1994**, *98*, 3809–3817.

(23) Tata, M.; John, V. T.; Waguespack, Y. Y.; McPherson, G. L. *J. Am. Chem. Soc.* **1994**, *116*, 9464–9470.

(24) Wüthrich, K. *NMR of Proteins and Nucleic Acids*; Wiley & Sons: New York, 1986.

(25) Croasmun, W. R.; Carlson, R. M. K. *Two-Dimensional NMR Spectroscopy: Applications for Chemists and Biochemists*, 2nd ed.; VCH: New York, 1994.

(26) Gippert, G. P.; Yip, P. F.; Wright, P. E.; Case, D. A. *Biochem. Pharm.* **1990**, *40*, 15–22.

(27) Kaptein, R.; Zuiderweg, E. R. P.; Scheek, R. M.; Boelens, R.; van Gunsteren, W. F. *J. Mol. Biol.* **1985**, *182*, 179–181.

(28) Clark, M.; Kramer, R. D.; VanOpdenbosch, M. J. *J. Comput. Chem.* **1989**, *10*, 982–1012.

(29) Blanco, M. *J. Comput. Chem.* **1991**, *12*, 237–247.

(30) Weiner, S. J.; Kollman, P. A.; Nguyen, D. T.; Case, D. A. *J. Comput. Chem.* **1986**, *7*, 230–252.

(18) Rusling, J. F.; Kumosinski, T. F. *J. Phys. Chem.* **1995**, *99*, 9241–9247.

(19) De, T. K.; Maitra, A. *Adv. Colloid Interface Sci.* **1995**, *59*, 95–193 and references therein.

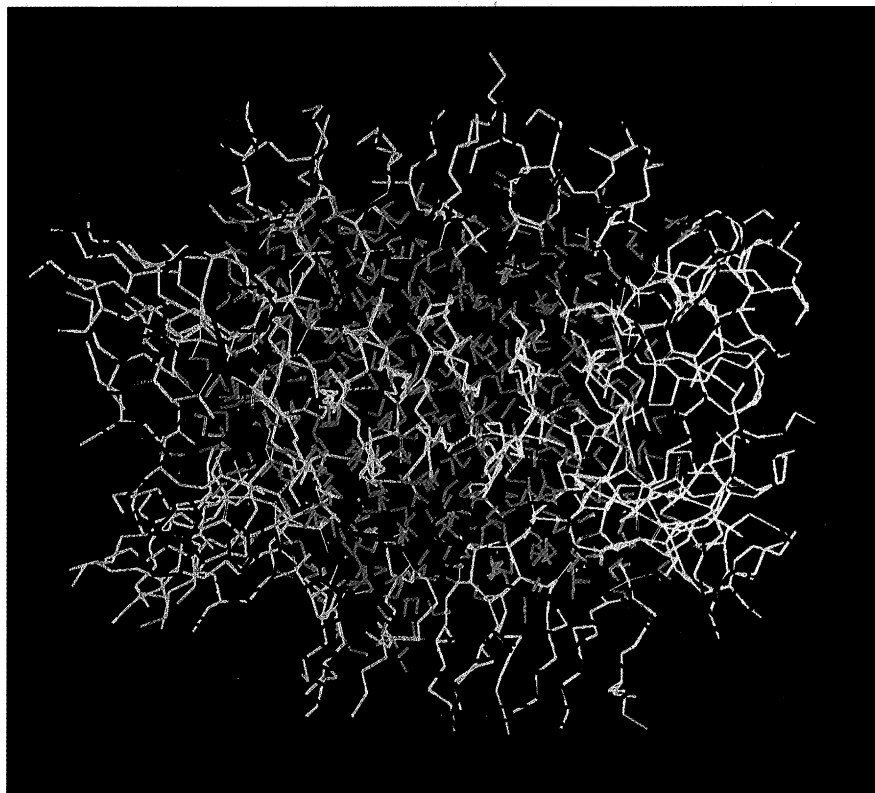


**Figure 1.** Result of dynamics simulation for a water/Aerosol-OT (AOT)/toluene microemulsion, including an empirical hydrophobic force for alkyl chains. The light-blue (cyan) interior of the aggregate represents the intact water droplet (401 molecules). The yellow surfactant tails (40 AOT monomer units) extend into the magenta oil phase (275 toluene molecules). The structures result from a 250 ps molecular dynamics simulation with simulated annealing from 500 to 300 K.

munication.<sup>31</sup> A united-atom approach was used for methyl and methylene groups in hydrocarbon chains, to reduce computation times. A cutoff value of 7 Å was utilized for all noncovalently bonded interactions. Molecular structures were energy minimized using a conjugate gradient algorithm. Energy minimizations were terminated when the energy difference between successive iterations was less than 0.1 kcal/mol.

**Molecular Dynamics Simulations.** All aggregate and biopolymer structures were initially energy minimized. Molecular dynamics simulations for each molecular structure or aggregate structure were carried out for 250 ps at 300 K, with a united-atom approach, both with and without solvent molecules. The stability of aggregate structures over the course of the dynamics simulations was determined by observing the following calculated parameters as a function of time: total potential energy ( $E_p$ ), radius of gyration ( $R_G$ ), and root-mean-square fluctuation ( $A$ ) of all atoms from the center of mass of the aggregate. Simulated annealing was used as a rigorous test of the stability of the dynamic structures. Simulated annealing tests were begun at a temperature of 500 K and lowered in 50 deg steps to 300 K over the course of 250 ps simulations. Constant densities for water and toluene were maintained within periodic boundaries for models when spheres (or cubes) of solvation were included. Hydrophobic attraction for alkyl chains was mimicked by scaling the van der Waals interaction term in the Tripos force field as previously described.<sup>18</sup>

**NMR Spectroscopy.** Poly(L-lysine) hydrobromide of molecular weight 3335 (average degree of polymerization (DP) = 16) was obtained from Sigma Chemical Co. (St. Louis, MO). The purity of polypeptide samples was checked using the Waters Pico-Tag amino acid analysis system, with automated gradient liquid chromatography (LC) analysis. Samples for NMR were dissolved in D<sub>2</sub>O at 25 mg/mL, and pD adjustments made using NaOD and/or DCl (Cambridge Isotopes, Andover, MA). A sample of pD 11.5 was diluted to 3.5 mM, and a sample of pD 8.6 was diluted to 2.5 mM (the observed pH of D<sub>2</sub>O solutions was converted

to pD by  $pD = pH + 0.4$ ).<sup>32</sup> One- and two-dimensional NMR spectra were obtained on a Varian Unityplus 400 spectrometer equipped with a 5 mm multinuclear, indirect detection probe. All homonuclear two-dimensional spectra were collected using hypercomplex data acquisition<sup>33</sup> to achieve quadrature detection in the indirectly detected dimension at a proton resonant frequency of 399.919 MHz. Acquisition parameters for two-dimensional experiments included the collection of 1024 complex points in the acquisition (F1) dimension and either 128 or 256 complex points in the evolution (F2) dimension. A spectral width of 2.2 kHz (5.5 ppm) was used in both dimensions. An average of 16–32 transients was obtained for average total experiment times of 4–8 h. An interactive Gaussian weighting function was used during processing. The evolution dimension was zero filled to 1024 points. Proton chemical shifts were referenced to internal acetone and corrected to tetramethylsilane (TMS). The following 2D spin-lock experiments were employed: total correlation spectroscopy (TOCSY),<sup>34</sup> rotating frame Overhauser effect spectroscopy (ROESY),<sup>35</sup> and transverse-ROESY (T-ROESY).<sup>36</sup> TOCSY experiments apply an MLEV-16 spin-lock,<sup>34</sup> and ROESY experiments apply a 30° Kessler spin-lock.<sup>35</sup> The transverse ROESY experiment employs a variable “windshield wiper” or Shaka-type spin-lock<sup>36</sup> to reduce the presence of spurious TOCSY peaks in the ROESY spectrum. Data processing was performed on a Sun Sparc-5 workstation using VNMR v.5.1 (Varian Associates) software.

Secondary structural features of poly(L-lysine) were also monitored by infrared spectroscopy using a Nicolet 740 FTIR spectrometer equipped with a Nicolet 660 data system. The sample chamber was purged with nitrogen prior to data collection. Each spectrum consisted of 4096 double-sided interferograms, co-added, phase-corrected, apodized (Happ-Genzel function), and

(32) Glascoe, P. K.; Long, F. A. *J. Chem. Phys.* **1960**, *64*, 188–190.

(33) States, D. J.; Haberkorn, R. A.; Ruben, D. J. *J. Magn. Reson.* **1982**, *48*, 286–292.

(34) Bax, A.; Davis, D. J. *Magn. Reson.* **1985**, *65*, 355–360.

(35) Kessler, H.; Griesinger, C.; Kerssebaum, R.; Wagner, R.; Ernst, R. R. *J. Am. Chem. Soc.* **1987**, *109*, 607–609.

(36) Hwang, T.-L.; Shaka, A. J. *J. Am. Chem. Soc.* **1992**, *114*, 3157–3159.

(31) Kumosinski, T. F.; Brown, E. M.; Farrell, H. M., Jr. *J. Dairy Sci.* **1993**, *76*, 931–945.

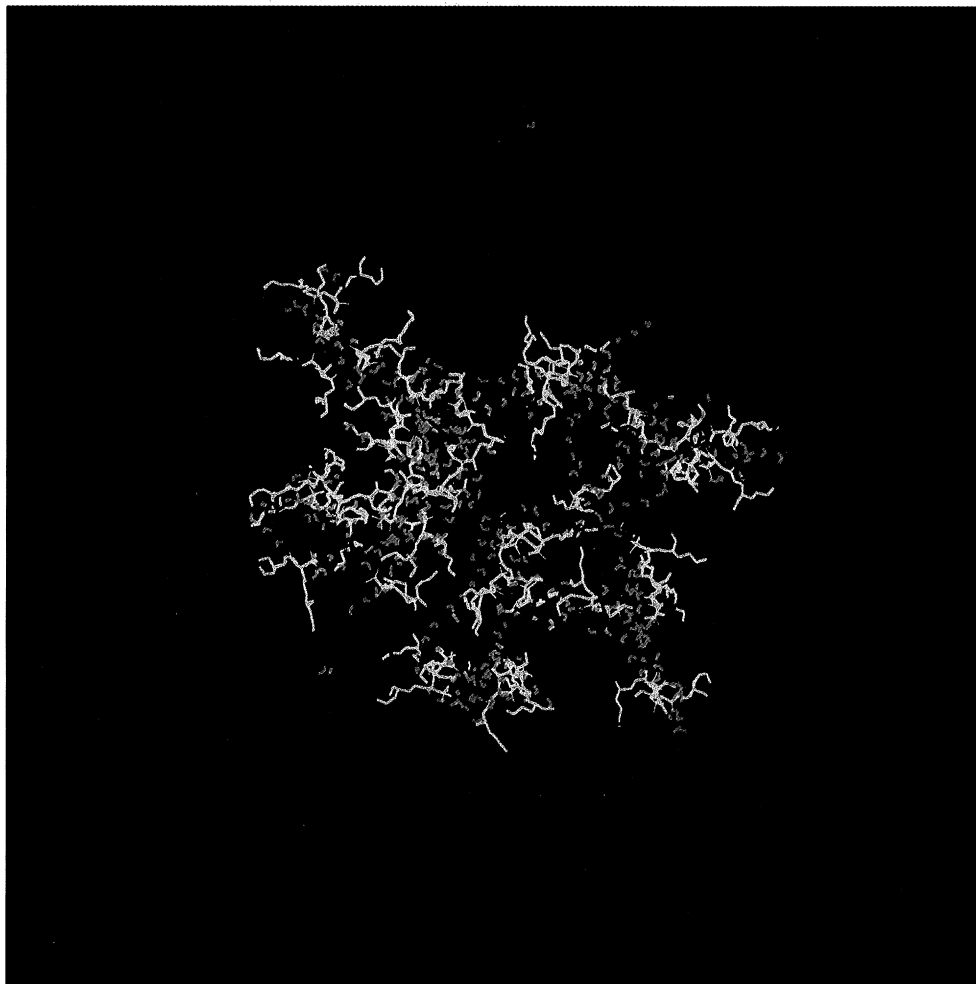


**Figure 2.** Result of dynamics simulation for the same water/Aerosol-OT (AOT)/toluene microemulsion as shown in Figure 1, without hydrophobic force. All other conditions for the dynamics simulation are the same as in Figure 1.

fast-Fourier transformed. Difference spectra were generated by subtraction of the D<sub>2</sub>O spectrum recorded under the same conditions as the sample spectra. Ultracentrifugation measurements were made on a Beckman Optima XL-A analytical ultracentrifuge, equipped with a removable high-intensity flash xenon light source/scanning monochromator and a UV-vis photoelectric detector. Poly(L-lysine) aggregation behavior was checked on the Beckman XL-A using the sedimentation equilibrium experiment. Peptide absorbance was monitored at 234 nm, as determined earlier from absorbance spectra obtained on a Beckman DU-7 UV-vis spectrophotometer.

## Results and Discussion

**Food Emulsions and Gels.** Food emulsions are often composite mixtures of lipids, proteins, emulsifiers, and water. Water-in-oil microemulsions (reversed micelles), which exist as thermodynamically stable, homogeneous single-phase solutions, can serve as simple model systems for studying the properties of food emulsions. The surfactant sodium bis(2-ethylhexyl)sulfosuccinate, or Aerosol-OT (AOT), which contains two branched hydrocarbon chains, can solubilize large amounts of water in the organic phase, without cosurfactant, depending on the surrounding nonpolar medium. A mixture of water/AOT/toluene forms a stable microemulsion, which has been used recently to promote polymerization of acrylamide.<sup>37</sup> However, no three-dimensional molecular predicted models of AOT assemblies have been developed via molecular modeling techniques. Molecular dynamics

simulations were used here to examine a variety of AOT assemblies and the effect of a long-range hydrophobic force *in vacuo* and in the presence of water and nonpolar solvents.

Micelle and reversed micelle structures with hydrocarbon tails in *all-trans* (or *anti*) conformations were energy minimized to arrive at initial aggregate structures. Molecular dynamics included simulated annealing performed on all systems to overcome local minima in the force field. Figure 1 shows the result of a 250 ps dynamics simulation on a microemulsion of AOT/water/toluene utilizing an empirical hydrophobic force. A multiplicative factor of 15 times the default van der Waals interaction term in the force field was used for hydrocarbon chains to simulate hydrophobic interaction, as previously discussed.<sup>18</sup> The invariance of the time dependence of the solute's radius of gyration, root-mean-square fluctuations of all atoms, and potential energy was used as a criterion for equilibrium (as was the case for all simulations shown hereinafter). A dynamic aggregate structure was maintained, with AOT polar head groups buried in the water droplet and alkyl chains extending into the toluene phase. Reversed micelles of low water to AOT ratio (less than or equal to 10) in toluene were more or less spherical, which is consistent with results from quasi-elastic light scattering (QELS) and small-angle neutron scattering (SANS) studies on similar AOT/water/alkane systems.<sup>38</sup> The result of an identical dynamics simulation on the same AOT/

(37) (a) Barton, J. *Macromol. Symp.* **1996**, *101*, 61–70. (b) Barton, J.; Stillhammerova, M. *Chem. Pap.—Chem. Vestni* **1996**, *50*, 41–44.

(38) Kotlarchyk, M.; Chen, S.-H.; Huang, J. S. J. *Phys. Chem.* **1982**, *86*, 3273–3276.

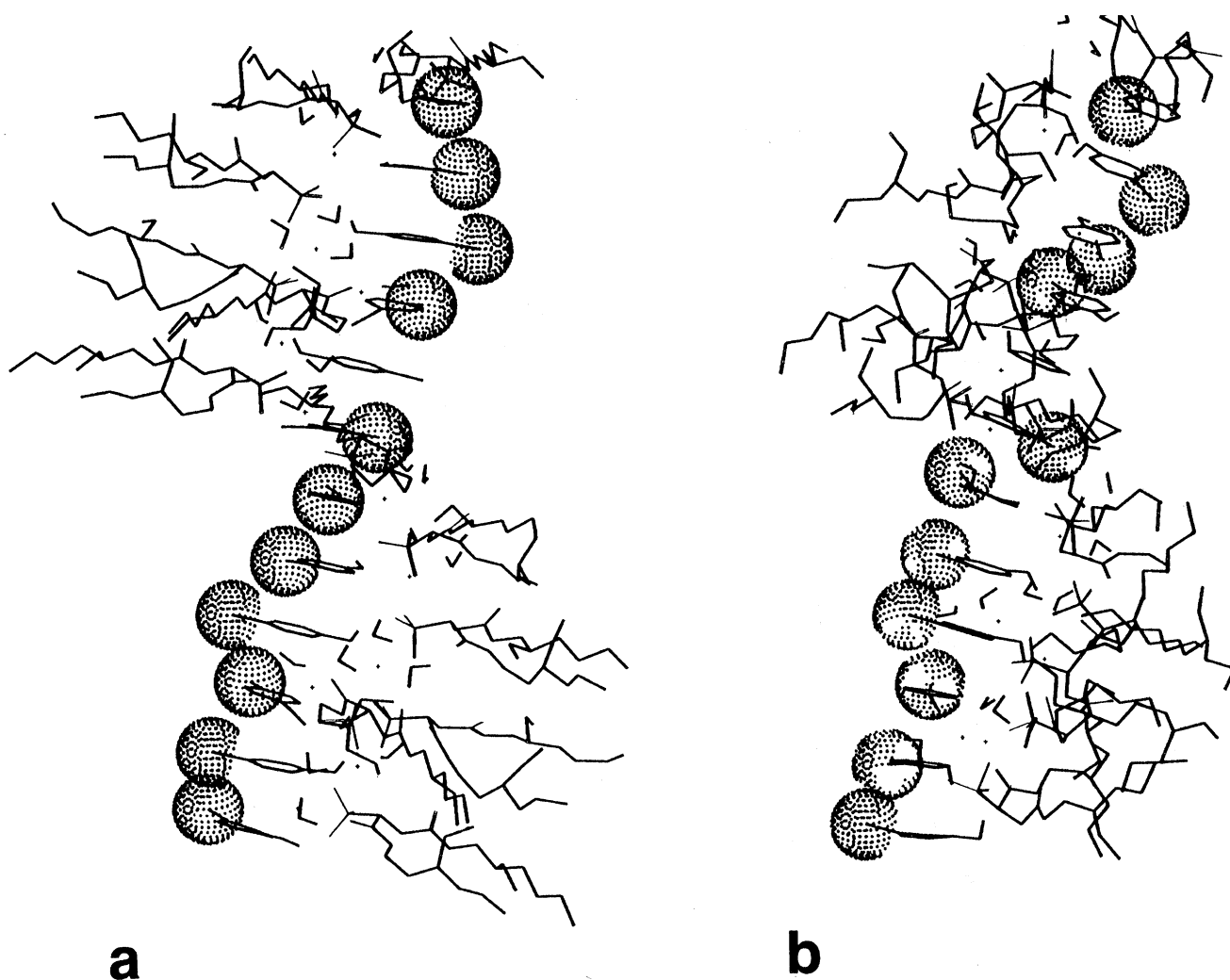


**Figure 3.** AOT/*para*-chlorophenol organogel: (a) initial structure with stacked phenols (spheres are phenolic chlorine atoms) and AOT hydrocarbon chains extending outward; (b) after 250 ps with hydrophobic force included.

water/toluene aggregate structure in the absence of a hydrophobic force for hydrocarbon chains is shown in Figure 2. The aggregate structure begins to “dissociate” over the course of the dynamics simulation at 300 K. The surfactant-coated water droplet has begun to fragment into smaller droplets, with increased dispersion into the toluene phase.

Similar results (not shown) were obtained for micelles of AOT in water. Dynamics simulations under conditions of simulated annealing yielded stable aggregate structures when the hydrophobic force was included. Ellipsoidal shapes were exhibited for structures of low aggregation number (10–15 monomer units), consistent with results from NMR diffusion measurements.<sup>39</sup> While shapes of the dynamic AOT micelle models were not consistent with a minimal spherical micelle, attempts at calculating an axial ratio(s) precluded the assignment of a specific nonspherical shape to the structures. Dynamics simulations of AOT micelles at 300 K without a hydrophobic force did not show structural stability. As was the case with the microemulsions, dynamics without some approximation to hydrophobic attraction of alkyl chains causes disruption of the assembled models and loss of structural equilibrium. During the course of the dynamics simulations for both the micelle and reversed micelle structures, many of the hydrocarbon tails developed

“kinks” as a result of *trans*-to-*gauche* isomerization. *Gauche* conformations of carbon–carbon bonds, which can induce fluidity in hydrocarbons, have been shown to play an important role in gel-to-liquid crystal phase transitions.<sup>18</sup>

Recently the formation of a novel organogel has been reported by addition of a variety of phenols to a solution of AOT in oil.<sup>21–23</sup> Unlike most surfactant- and polymer-based gels, these gels form at very small concentrations of low molecular weight precursors (AOT and phenols) in a diversity of nonpolar solvents. It has been speculated that the exceptional sensitivity of these gels to temperature and moisture could lead to use in sensing devices as well as in templating the synthesis of inorganic microstructures. In the proposed gel structure, phenol molecules are stacked to form a strand, with hydrogen-bonding associations between the phenols and the polar sulfosuccinate headgroup of the surfactant. Energy-minimized structures were obtained for a stacked AOT/*para*-chlorophenol gel in CCl<sub>4</sub>, in benzene, and *in vacuo*. Figure 3 shows the results of a dynamics simulation on an energy-minimized gel structure including a hydrophobic force. The left hand side shows the initial structure with surfactant molecules arranged around a column of stacked phenols in a “spiral staircase” arrangement. The right hand side shows the result of a 250 ps *in vacuo* molecular dynamics simulation at 300 K. While there has been some redistribution of the packing of alkyl chains, the integrity

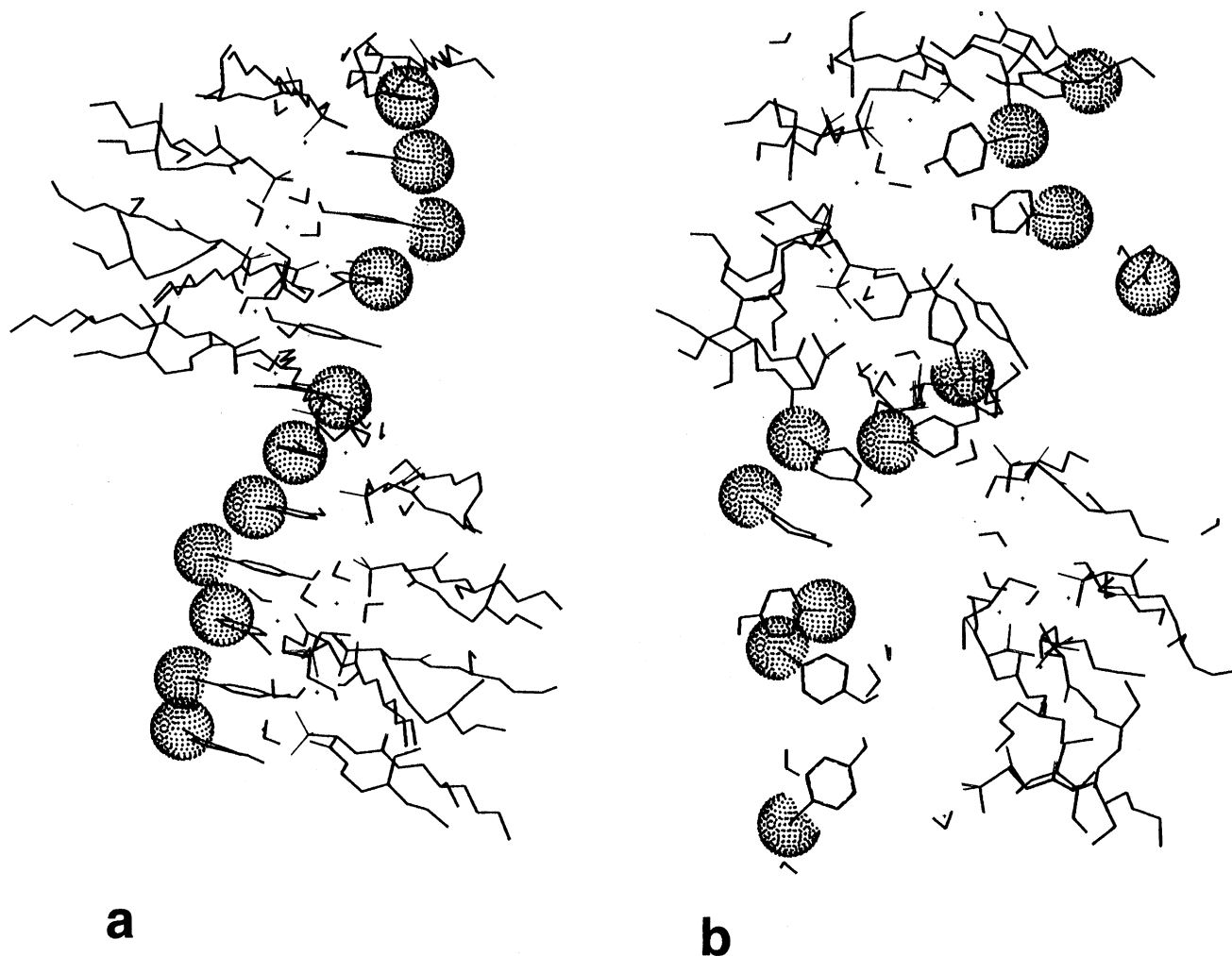


**Figure 4.** AOT/*para*-chlorophenol organogel: (a) initial structure with stacked phenols (spheres are phenolic chlorine atoms) and AOT hydrocarbon chains extending outward; (b) after 1.5 ps with no hydrophobic force.

of the gel structure is maintained throughout the dynamics simulation. Similar results were obtained when either  $\text{CCl}_4$  or benzene solvent molecules were included. As NMR results reveal gel melting above  $30^\circ\text{C}$  (303 K),<sup>22</sup> simulated annealing above 300 K was not attempted. Figure 4 shows an example of the same dynamics simulation on the same organogel system without any adjustment in the force field to account for hydrophobic attraction of the AOT tails. On the left is the initial energy-minimized structure. At 300 K (no simulated annealing) the ordered structure begins to fall apart after just 1.5 ps, as seen on the right side of Figure 4. Similar results were obtained when nonpolar solvent was included. While the stacking arrangement of surfactant tails remains at the level of speculation, molecular modeling results indicate that interchain hydrophobic forces play a role in stabilizing AOT/phenol organogels. Similar forces are likely significant in maintaining the stability of gels and emulsions in food colloids and dispersions.

**NMR and Modeling of Polylysine.** Poly(L-lysine) has often been considered as a simple model for native proteins, as at least three forms, random coil,  $\alpha$ -helix, and  $\beta$ -sheet, can be observed in aqueous solution depending upon pH and temperature. The secondary structural dependence upon pH has been extensively characterized by a wide variety of techniques including circular dichroism (CD), infrared (FTIR), Raman, and NMR spectroscopic methods. Coagulation and gelation of globular food proteins commonly determine many of the resultant properties of food materials. It has been widely held that

protein gelation and/or precipitation arises from alignment of unfolded peptide chains and subsequent formation of extensive regions of intermolecularly cross-linked  $\beta$ -sheets. Intermolecular interactions involving hydrophobic groups may play a considerable role in driving these physical processes. Consequently, poly(L-lysine) serves as an effective model for studying the influence of hydrophobic groups in peptide conformational changes and aggregation.

Poly(L-lysine) undergoes a random coil–helix transition upon deprotonation of the aminobutyl side chain around pH 10.6 (pD 11), the pH dependence of which has been well characterized by  $^{13}\text{C}$  NMR chemical shifts and longitudinal ( $T_1$ ) relaxation.<sup>40</sup> At high pH ( $>10.5$ ) there exists a temperature dependent  $\alpha$ -helix  $\leftrightarrow$   $\beta$ -sheet equilibrium, which has been investigated by CD and  $^{13}\text{C}$  NMR.<sup>41</sup> Figure 5 shows the 1D  $^1\text{H}$  spectra of poly(L-lysine) in  $\text{D}_2\text{O}$  at (a) pD 8.6 and  $30^\circ\text{C}$ , (b) pD 11.5 and  $30^\circ\text{C}$ , and (c) pD 11.5 and  $4^\circ\text{C}$ . It has been reported that nearly pure  $\alpha$ -helix or  $\beta$ -sheet conformations can be obtained if the temperature is maintained below  $4^\circ\text{C}$  or above  $50^\circ\text{C}$ , respectively.<sup>42</sup> Figure 5A represents a typical NMR spectrum of the polypeptide in a random coil (or possibly extended helix) conformation, Figure 5B the concomitant

(40) Saitô, H.; Smith, I. C. P. *Arch. Biochem. Biophys.* **1973**, *158*, 154–163.

(41) Wittebort, R. J.; Szabo, A.; Gurd, F. R. N. *J. Am. Chem. Soc.* **1980**, *102*, 5723–5728.

(42) Bradbury, E. M.; Crane-Robinson, C.; Goldman, H.; Rattle, H. W. E. *Biopolymers* **1968**, *6*, 851–862.

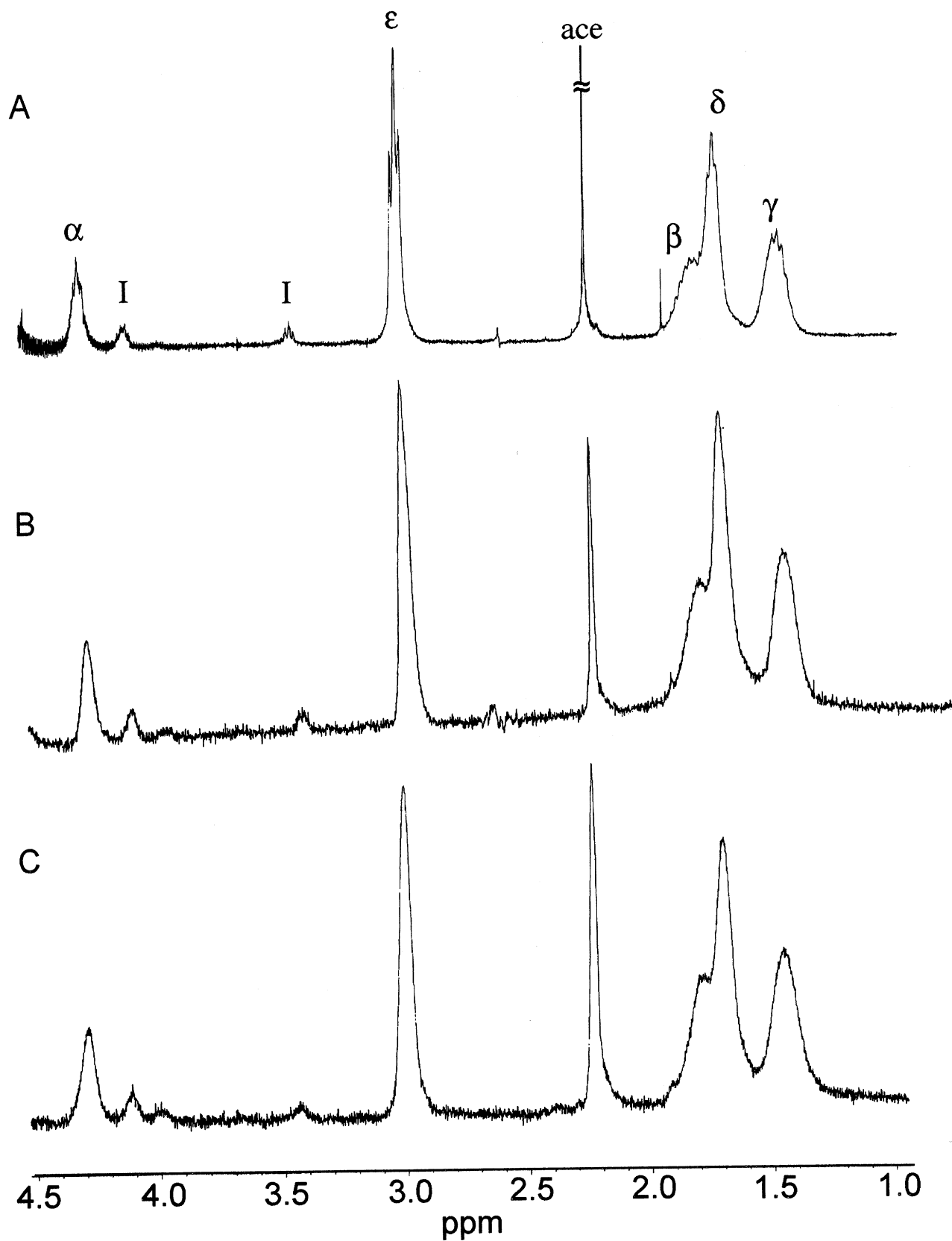


**Figure 5.**  $^1\text{H}$  spectra of poly(L-lysine) in  $\text{D}_2\text{O}$ : (A) pD 8.6, 30 °C; (B) pD 11.5, 30 °C; (C) pD 11.5, 4 °C. Imp = impurity (sample impurities were identified as no more than 2% residual free amino acid (not lysine), as determined by amino acid analysis involving hydrolysis, precolumn derivatization, and automated gradient reverse phase HPLC).

resonances for helix and sheet, and Figure 5C the polypeptide in primarily  $\alpha$ -helical form. The pH dependent conformations of poly(L-lysine) were confirmed by FTIR spectroscopic measurements. Absorption spectra for pD 6.9 (below the side chain  $\text{pK}_a$ ) and pD 11.5 poly(L-lysine)

were obtained at 30 °C and compared to previously reported FTIR results.<sup>43</sup> Analysis of the amide I and amide

(43) Jackson, M.; Harris, P. I.; Chapman, D. *Biochim. Biophys. Acta* 1989, 998, 75–79.

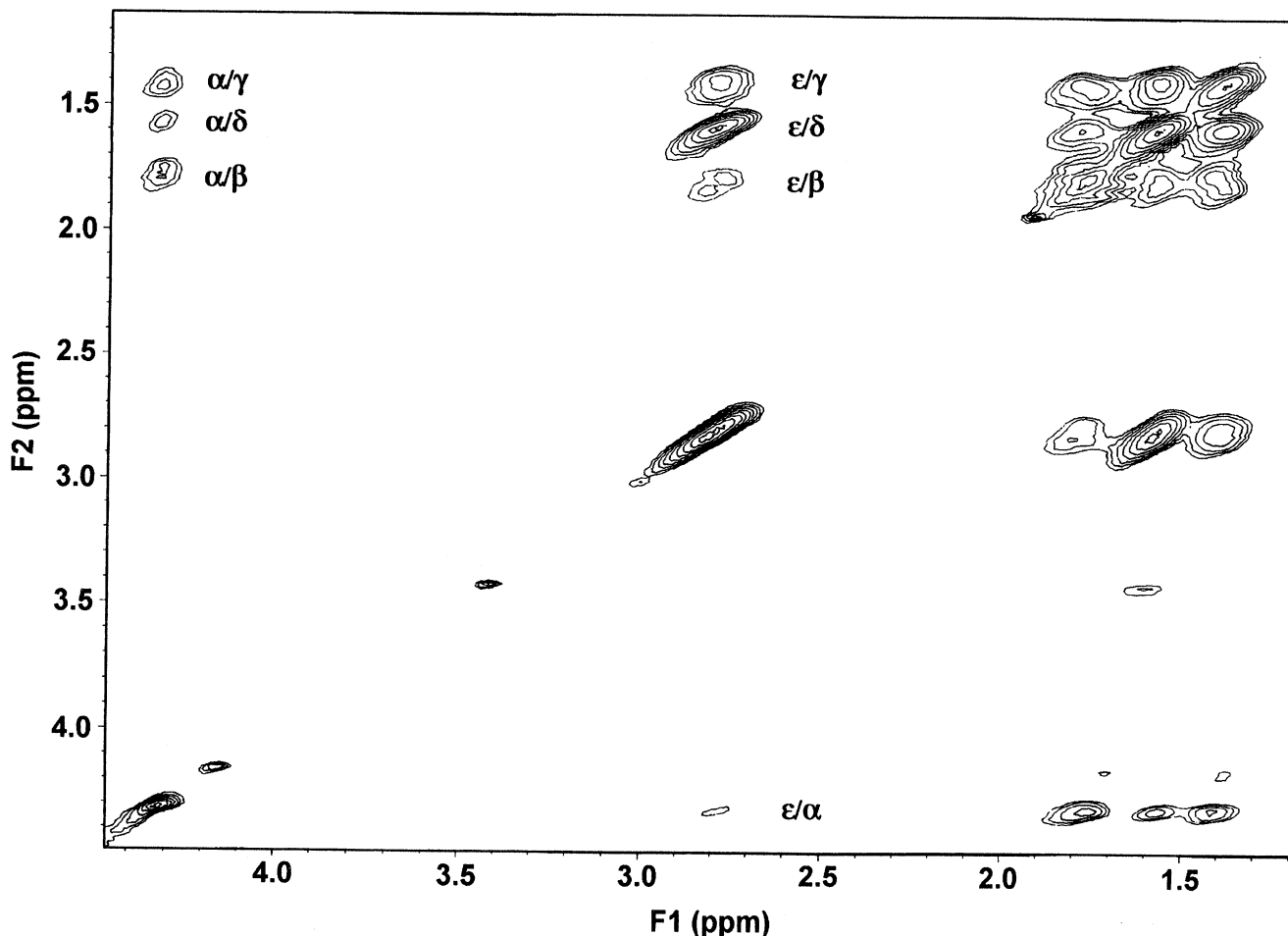


**Figure 6.** TOCSY spectrum of pD 11.5 poly(L-lysine) at 30 °C with a mix time of 60 ms. The major spin system  $J$  couplings are indicated (e.g., the  $C_\alpha$  to  $C_\beta$  proton coupling is labeled as  $\alpha/\beta$ ).

**Table 1.**  $^1\text{H}$   $T_1$  Values for Poly(L-Lysine)<sup>a</sup>

sample	$T_1$ value (s)			
	$C_\alpha$	$C_\gamma$	$C_\delta$	$C_\epsilon$
pD 8.6, $T = 30\text{ }^\circ\text{C}$	0.672 (0.072)	0.346 (0.029)	0.500 (0.019)	0.818 (0.021)
pD 11.5, $T = 30\text{ }^\circ\text{C}$	0.811 (0.058)	0.391 (0.014)	0.527 (0.008)	0.839 (0.018)
pD 11.5, $T = 4\text{ }^\circ\text{C}$	0.904 (0.016)	0.357 (0.004)	0.403 (0.003)	0.528 (0.003)

<sup>a</sup> The standard error of calculation is in parentheses. Values are not calculated for  $C_\beta$ .

**Table 2.**  $^1\text{H}$   $T_2$  Values for Poly(L-Lysine)<sup>a</sup>

sample	$T_2$ value (s)			
	$C_\alpha$	$C_\gamma$	$C_\delta$	$C_\epsilon$
pD 8.6, $T = 30\text{ }^\circ\text{C}$	18.9 (3.7)	53.7 (2.4)	42.8 (2.3)	20.2 (3.0)
pD 11.5, $T = 30\text{ }^\circ\text{C}$	17.8 (3.1)	49.9 (2.4)	40.8 (2.2)	23.1 (1.6)
pD 11.5, $T = 4\text{ }^\circ\text{C}$	63.4 (1.3)	47.6 (2.5)	61.8 (6.8)	66.4 (13)

<sup>a</sup> The standard error of calculation is in parentheses. Values are not calculated for  $C_\beta$ .

II bands for pD 6.9 poly(L-lysine) showed a single strong band at  $1644\text{ cm}^{-1}$ , corresponding to random structures. The spectrum of pD 11.5 poly(L-lysine) at  $30\text{ }^\circ\text{C}$  contained bands corresponding to  $\beta$ -sheet ( $1611, 1680\text{ cm}^{-1}$ ) and a strong signal at  $1640\text{ cm}^{-1}$ , which may correspond to an overlap of the reported signals for  $\alpha$ -helix ( $1638\text{ cm}^{-1}$ ) and random coil ( $1644\text{ cm}^{-1}$ ). A low temperature ( $4\text{ }^\circ\text{C}$ ) FTIR measurement of pD 11.5 poly(L-lysine) was not successfully completed at the time of this study.

The random coil structure in Figure 5A appears to have a higher degree of mobility, as reflected in greater spectral resolution with respect to that observed in Figure 5B and C. This is the case for both the peptide backbone ( $C_\alpha$  protons) and side chains (e.g.  $C_\epsilon$  protons). Previous studies<sup>42</sup> have shown that for a large poly(L-lysine) peptide (degree of polymerization = 688), proton NMR signals broaden significantly at pD values above 10.2, which may be due in part to aggregation effects. While the small measure resonant line broadening at high pD indicates some degree of motional restriction upon formation of periodic secondary structure, the magnitude of broadening effects for this small peptide (DP = 16) does not imply substantial aggregation of peptide monomers. Chemical shift values for the random coil (pD 8.6) structure closely match those reported for a similar sample (pD 7,  $T = 77\text{ }^\circ\text{C}$ ) of a larger poly(L-lysine) with an average degree of polymerization of 140 units.<sup>44</sup> Very little change in  $^1\text{H}$  chemical shift is observed for the high pD samples in Figure 5B and C. Several factors might account for this. The low degree of polymerization (16 monomer units) may preclude the complete formation of stable helices and sheets. Ordered structures may be in equilibrium with extended, aperiodic structure. Additionally, reported average chemical shift values for protein and peptide backbone protons in random coil structures fall midway between average values for  $\alpha$ -helix (upfield chemical shift) and  $\beta$ -sheet (downfield) structures.<sup>24</sup> The acknowledged  $\alpha$ -helix  $\leftrightarrow$   $\beta$ -sheet equilibrium for this polypeptide may

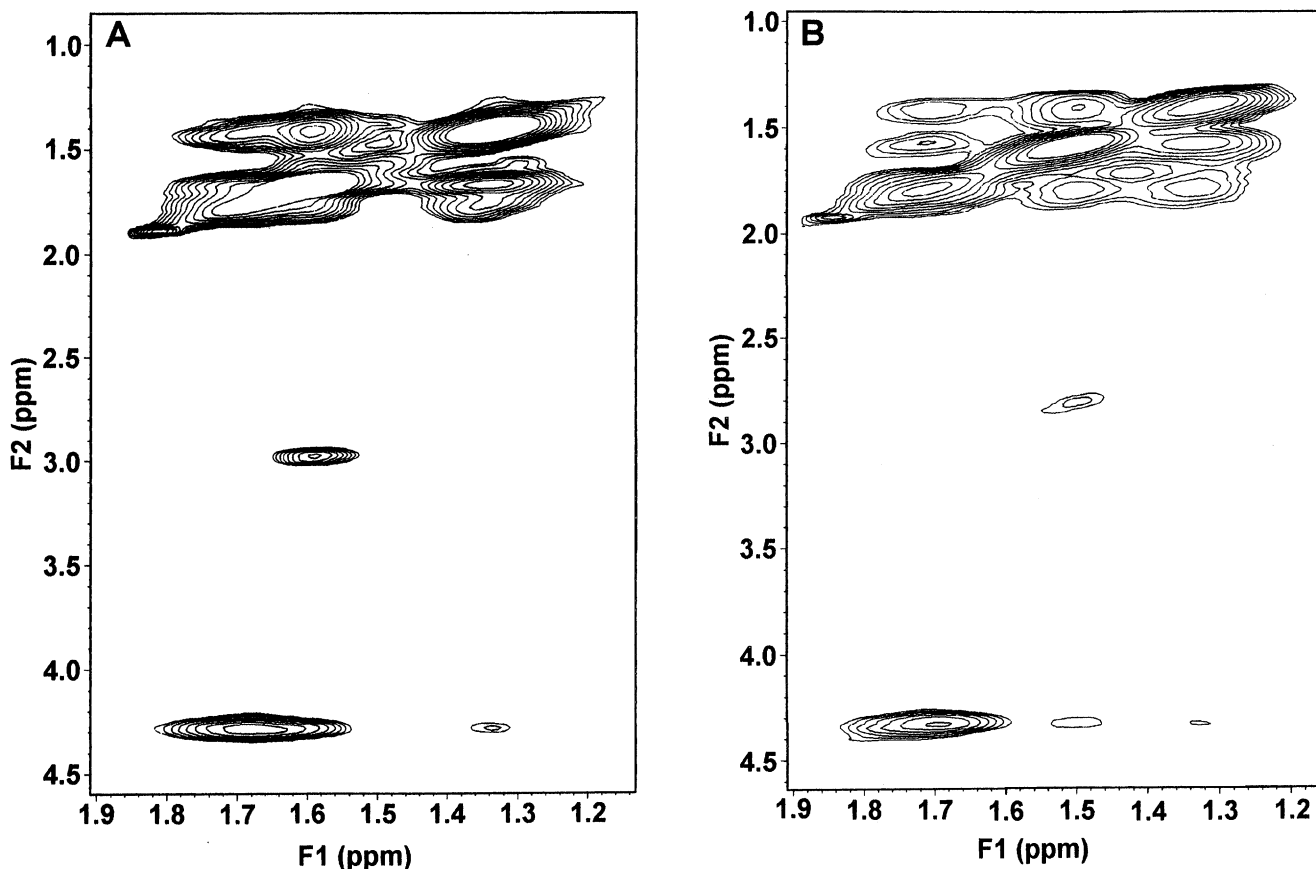


**Figure 7.** Region of poly(L-lysine) ROESY spectra showing side chain Overhauser couplings: (A) pD 8.6,  $T = 30\text{ }^{\circ}\text{C}$ , mix time = 60 ms; (B) pD 11.5,  $T = 30\text{ }^{\circ}\text{C}$ , mix time = 60 ms.

give a time-averaged resonance similar to that of the random coil, particularly for backbone protons.

High-resolution two-dimensional (2D)  $^1\text{H}$  NMR can furnish structural information with regard to the *three-dimensional* conformational space of the molecule. 2D NMR techniques offer a number of significant enhancements with respect to traditional 1D techniques, including spectral resolution of highly overlapped resonances. Two-dimensional  $J$ -spectroscopies, such as TOCSY, allow resolution of scalar (through-bond) spin couplings and facile assignment of chemical shifts. Overhauser effect methods, such as ROESY, offer spatial information which can be used to identify protons separated by less than 5 Å. Homonuclear scalar couplings of the lysine residue spin system were determined by TOCSY. ROESY and transverse-ROESY techniques were used to distinguish poly(L-lysine) side chain/backbone interactions by measuring through-space couplings of alkyl protons. Figure 6 shows the TOCSY spectrum of pD 11.5 poly(L-lysine) at room temperature ( $30\text{ }^{\circ}\text{C}$ ) with a mix time of 60 ms. In all TOCSY experiments, with mix times of 60–120 ms, the entire spin system of nonlabile protons was observable, i.e. the backbone  $\text{C}_\alpha$  proton coupled to each moiety along the side chain outward to the  $\text{C}_\epsilon$  protons. Exchangeable protons from backbone amide and side chain amine groups were not observable in  $\text{D}_2\text{O}$  solution. Although chemical shift assignments were made by way of 1D spectra, assignment of the TOCSY spectrum provides evidence of scalar cross peaks which can potentially show up as artifacts in Overhauser experiments.

Figure 7A shows an expansion of the ROESY spectrum of pD 8.6 poly(L-lysine) at room temperature ( $30\text{ }^{\circ}\text{C}$ ) with a mix time of 60 ms. Side chain methylene protons ( $\text{C}_\beta$  through  $\text{C}_\delta$ ) are strongly coupled to one another, with  $\text{C}_\delta$  moderately coupled to  $\text{C}_\epsilon$ . This may indicate a partially

coiled (higher *gauche-trans* ratio) conformation of the hydrocarbon portion of the chain, possibly to reduce water-hydrocarbon contact. Backbone  $\text{C}_\alpha$  protons appear strongly coupled to  $\text{C}_\beta$  protons, although much of this cross peak intensity was shown to be TOCSY interference (*vide infra*). Figure 7B shows a similar expansion of the ROESY spectrum of pD 11.5 poly(L-lysine) at  $30\text{ }^{\circ}\text{C}$  (mix time 60 ms). Again, strong methylene couplings are observed. Since buildup rates of cross peak intensity, which are used to derived internuclear distances, were not determined, changes in side chain conformation at high pD cannot be directly quantitated. The transverse-ROESY experiment was used to establish whether coherent magnetization transfer by TOCSY was yielding spurious cross peaks in the ROESY spectra of the poly(L-lysine) samples. The T-ROESY spectra of pD 8.6 and pD 11.5 poly(L-lysine) at  $30\text{ }^{\circ}\text{C}$  (not shown) both exhibited similar methylene proton couplings to those observed from ROESY. Couplings of backbone  $\text{C}_\alpha$  protons to side chain methylene protons were greatly diminished in the T-ROESY spectrum, indicating that the various  $\text{C}_\alpha$  couplings observed in Figure 7 originated from  $J$ -coupling pathways.

The ROESY spectrum of pH 11 poly(L-lysine) at  $4\text{ }^{\circ}\text{C}$  (ostensibly all  $\alpha$ -helix) did not show any couplings of  $\text{C}_\alpha$  protons to other protons. Attenuation of ROESY cross peaks may be due in this case to changes in the isotropic rotational correlation time  $\tau_c$  of the molecule as a function of reduced temperature and/or peptide disaggregation. The solution aggregation behavior of the peptide was confirmed by analytical ultracentrifugation. The sedimentation equilibrium measurement of poly(L-lysine) in  $\text{D}_2\text{O}$  at pH 11.5 indicates a concentration dependent association of peptides at  $30\text{ }^{\circ}\text{C}$ . The transition from monomer to higher order aggregates occurred at peptide concentrations of 4.0–5.0 mg/mL. The sedimentation

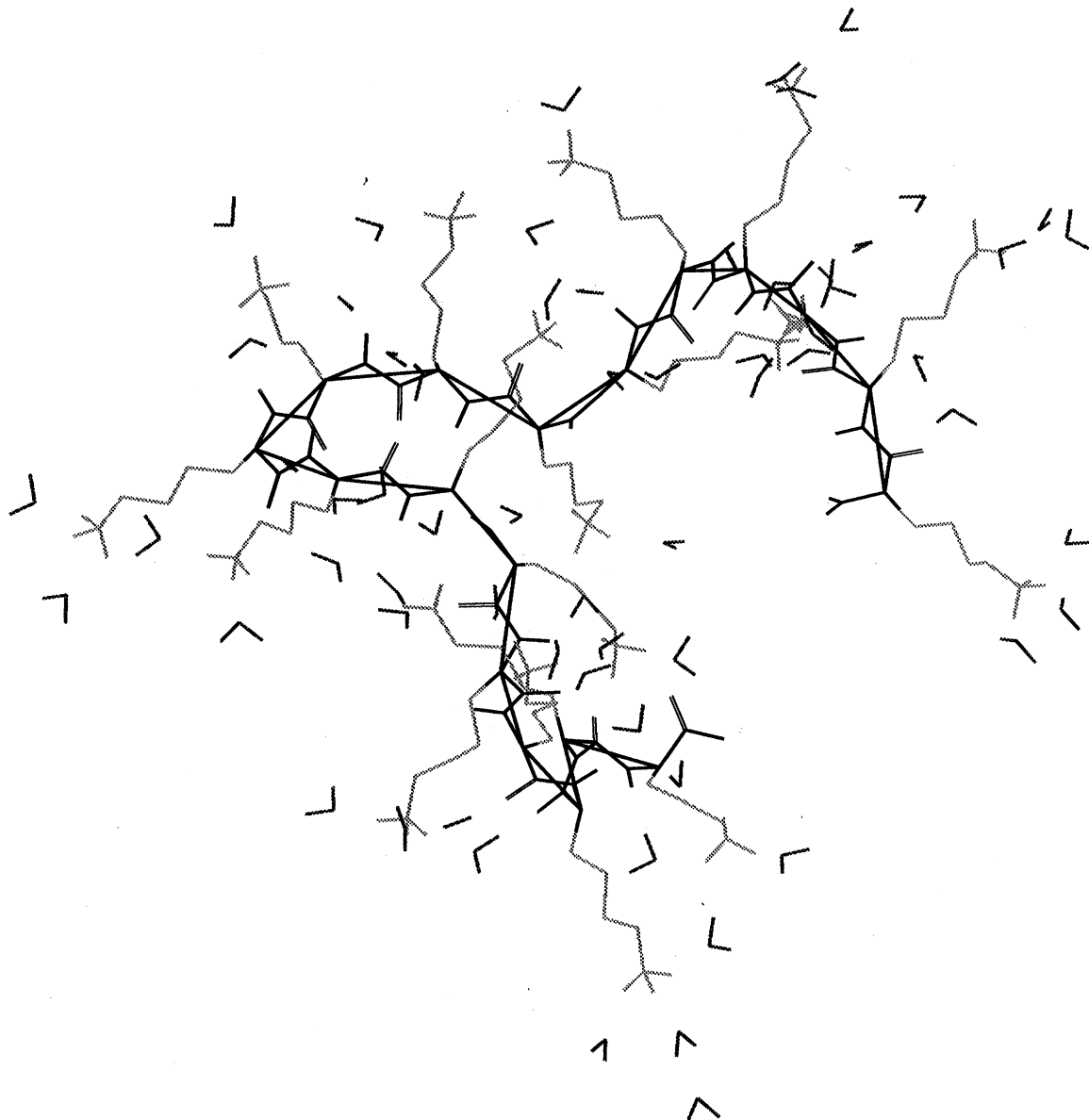


**Figure 8.** Result of 250 ps dynamics simulation with simulated annealing on charged poly(L-lysine) in water with hydrophobic force included. The backbone (with  $\alpha$ -carbon trace) and water molecules are in dark black, and the side chain groups are in dark gray.

equilibrium measurement of the same poly(L-lysine) sample at 4 °C indicated the presence of only monomer. No association of peptide was observed at 4 °C for measurements made at 5 and 19 h in the centrifugal force field. A sedimentation equilibrium study of the temperature dependent association of bovine  $\beta$ -casein showed a similar monomer- $n$ -mer association scheme.<sup>45</sup> Monomer was observed at 2 °C, and higher order aggregates were observed at temperatures approaching 30 °C. Both the poly(L-lysine) and  $\beta$ -casein results are consistent with hydrophobically driven self-association.

Spin-lattice ( $T_1$ ) and spin-spin ( $T_2$ ) relaxation measurements are important in microdynamical studies, providing information on internal motion, molecular diffusion, and chemical exchange. Magnetization transfer between abundant nuclei such as protons is often efficient enough to lead to a single relaxation time constant for all protons in the spin system. This phenomenon, called spin diffusion, can diminish the dynamical information

obtained from proton relaxation measurements. However, the contribution of vicinal protons to the relaxation of methylene protons in poly(L-lysine) is appreciably reduced by rotation about the C-C bonds,<sup>43</sup> giving rise to a heterogeneity of side chain proton  $T_1$  relaxations. Table 1 shows the proton  $T_1$  values calculated for poly(L-lysine) under various conditions in this study. Table 2 shows the proton  $T_2$  values calculated for the same samples. At room temperature ( $T = 30$  °C) there is minimal-to-no statistical change in the  $T_1$  and  $T_2$  values calculated for poly(L-lysine) methylene protons at pD 11.5 versus pD 8.6. This suggests little restriction of side chain mobility upon formation of secondary structure. In comparison of the same two data sets, backbone  $C_\alpha$  protons show an increase in  $T_1$  and a small decrease (although statistically marginal) in  $T_2$ . An increase in  $T_1$  and decrease in  $T_2$  may be attributed to a small increase in the molecular correlation time  $\tau_c$  upon formation of periodic secondary structure (for values of  $\tau_c$  less than  $\sim 10^{-9}$  s, i.e. below the  $T_1$  minimum,  $T_1$  is directly proportional and  $T_2$  indirectly proportional to  $\tau_c$ ). However, as with 1D NMR line widths and 2D ROESY cross

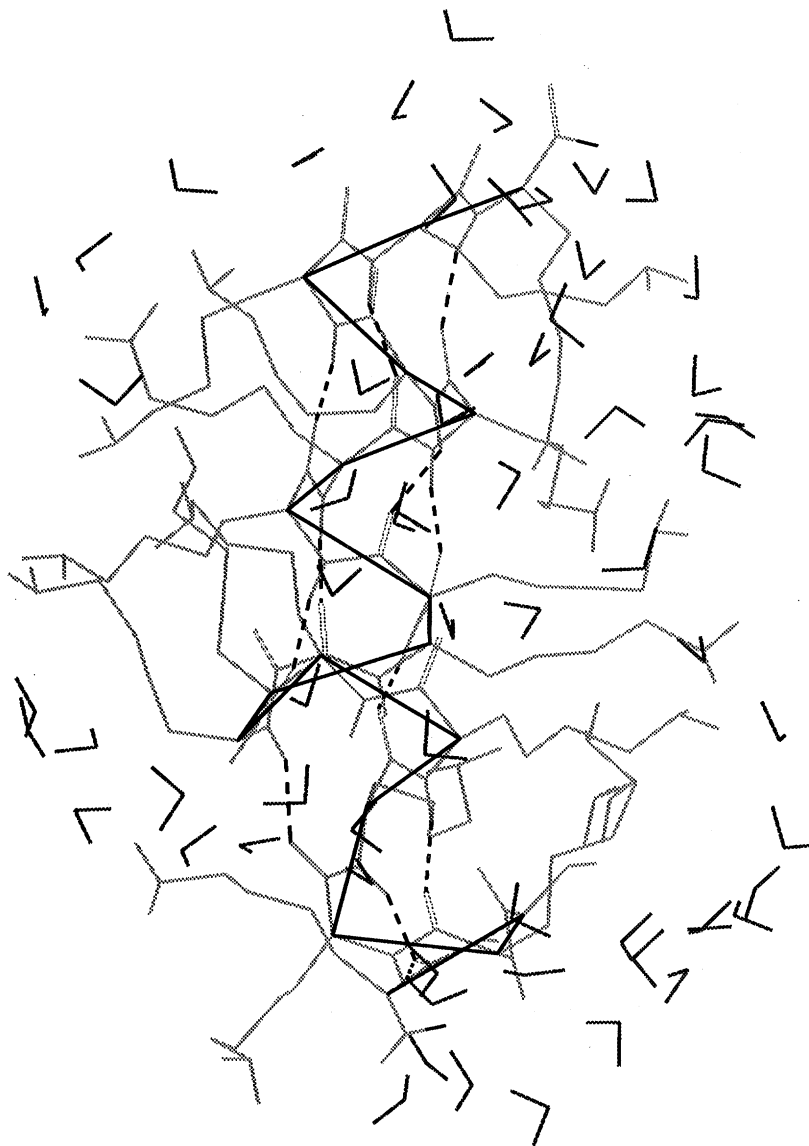


**Figure 9.** Result of 250 ps dynamics simulation at 278 K on deprotonated,  $\alpha$ -helical poly(L-lysine) in water with hydrophobic force included. The backbone and water molecules are in dark black ( $\alpha$ -carbon trace and intrachain hydrogen bonds included), and the side chain groups are in dark gray.

peaks,  $T_1$  and  $T_2$  measurements suggest only a minimal change in the quasi-isotropic motion of the polymer backbone.

Although lysyl side chains appear to have a good deal of independent motion in  $\beta$ -sheet and/or  $\alpha$ -helical forms of poly(L-lysine), the hydrophobicity of the butyl portion of the side chain may be influential in stabilizing the secondary structure of the peptide. Molecular dynamics simulations were used to determine the role of side chain hydrophobicity in governing the structural and functional properties of peptide and peptide aggregate structures. Figure 8 shows the result of a 250 ps dynamics simulation on a charged poly(L-lysine) structure in water utilizing a hydrophobic force approximation of 15 times the default van der Waals interaction term in the force field for united atom  $\text{CH}_x$  groups. The initial structure, prior to dynamics simulation, was built in a fully extended form, with charged side chains extending perpendicular to the backbone. With the hydrophobic approximation in place, the peptide adopted a semirandom extended helical form, as was suggested on the basis of CD results.<sup>41</sup> The side chain groups in Figure 8 appear somewhat kinked. The formation of partial gauche conformations for carbon-carbon rotamers may explain the through-space coupling

of methylene protons in the ROESY spectra. In the absence of a hydrophobic potential, the dynamic peptide structure remained in a fully extended form, with electrostatic repulsions dominating the side chain conformation.

Hydrophobic interactions play an even more important role in stabilizing  $\alpha$ -helical structures at high pH. Figure 9 shows the result of a 250 ps dynamics simulation on an  $\alpha$ -helical poly(L-lysine) structure in water utilizing a similar hydrophobic force. Although pH was not specified on the basis of a change in the nature of the solvent, the initial peptide structure contained side chains in their deprotonated, uncharged form. Hydrogen bonds between backbone N-H and C=O groups were also included in the initial structure. The helical structure was maintained throughout the dynamics simulation at 278 K (5 °C), including helix-stabilizing hydrogen bonds. Side chains appear extended but somewhat kinked, as in the coil structure in Figure 8. This result is supported by the lack of change in the side chain proton  $T_1$  or  $T_2$  between pD 8.6 and pD 11.5 poly(L-lysine). In the absence of the hydrophobic approximation, the helical structure is not maintained. The structure begins to uncoil after a few picoseconds, with breaking of interresidue hydrogen bonds

and full extension of the backbone. Since no side chain electrostatic forces are present to drive this conformational change, it is concluded that hydrophobic forces are necessary in stabilizing secondary structures of poly(L-lysine).

The approximation to hydrophobic attraction used in the Tripos force field simply increases the minimum potential energy in the Lennard-Jones (6–12) potential, which is used to simulate van der Waals nonbonded interactions. This is a rather crude approximation which has shown some limitations. Initial studies<sup>18</sup> involved simulating the aggregation of simple amphiphile systems such as monolayers, bilayers, and small micelles. The approximation has proven effective here on a number of larger systems like three-component microemulsions, surfactant organogels, and small peptides. However, in an attempt to simulate larger supramolecular structures, the model has revealed some inadequacies. A small number ( $n = 3-6$ ) of 16-residue poly(L-lysine) monomers in sheetlike configurations were docked in attempts to model the conditions necessary for protein gelation. The hydrophobic force as used in previous models was not sufficient to hold together a multicomponent aggregate, with the hydrogen bonding associations necessary for three-dimensional  $\beta$  pleated sheets. This is a significant limitation in the model, considering that self-supporting protein gels usually require a molecular weight average per protomer of tens of thousands of daltons.

### Conclusions

The physical nature of hydrophobic attractive forces remains as yet ambiguous. One clear fact is that hydrophobic forces influence the functionality of foods and food proteins, including emulsifying ability, foaming capacity, and thermally induced coagulation and gelation. Commercial molecular modeling software packages do not include a potential in the force field to account for hydrophobic attraction of hydrocarbon groups. The approximation used in this study has proven to be essential in modeling a number of dynamic aggregate systems,

which have been previously well-characterized by experimental methods. The limitation in this simple approximation lies in modeling the very long-range (10–60 nm or more) weak forces measured experimentally. The inclusion of a new potential in the Tripos force field which allows for long-range exponential dispersion forces may be necessary for modeling large supramolecular aggregates, such as cross-linked  $\beta$ -sheet regions in protein gels.

A variety of analytical methods from NMR spectroscopy have allowed for the assessment of conformational changes in the model peptide poly(L-lysine). One-dimensional <sup>1</sup>H NMR chemical shifts and line widths indicate that the segmental mobility of the poly(L-lysine) backbone is not greatly attenuated by the formation of periodic secondary structure at high pD. Through-space couplings from ROESY and T-ROESY measurements suggest that, while lysyl side chain mobility remains largely unrestricted upon formation of  $\alpha$ -helix or  $\beta$ -sheet structures, motional anisotropy does increase as one moves along the chain closest to the backbone. These conclusions are supported by  $T_1$  and  $T_2$  relaxation studies.

The conformational information obtained for alkyl chain regions is noteworthy in that local molecular structure has been shown previously<sup>7,8</sup> to govern the magnitude of measured hydrophobic attractive forces. These forces play a role in stabilizing secondary structural domains of poly(L-lysine), as supported by molecular modeling and dynamics studies. The combined use of molecular modeling and NMR spectroscopic methods allows for a multi-approach analysis of the forces involved in macromolecular interactions, which will lead to a better understanding of the diverse functional properties of foods.

**Acknowledgment.** The authors wish to thank Mr. Joseph Unruh for assistance with FTIR measurements, Dr. Gregory King for assistance with molecular modeling experiments, and Dr. Harold Farrell for helpful discussions and assistance with ultracentrifugation measurements.